

Precise estimation of spin drift velocity and spin mobility in the absence of synthetic Rashba spin-orbit field in a Si metal-oxide-semiconductor

Hajime Inoue,¹ Hayato Koike,² Ryo Ohshima ,^{1,3} Yuichiro Ando,^{1,3,4} and Masashi Shiraishi ^{1,3}

¹*Department of Electronic Science and Engineering, Kyoto University, Kyoto 615-8510, Japan*

²*Advanced Products Development Center, TDK Corporation, Ichikawa, Chiba 272-8558, Japan*

³*Center for Spintronics Research Network, Kyoto University, Uji 611-0011, Japan*

⁴*JST-PRESTO, Kawaguchi, Saitama 332-0012, Japan*



(Received 18 September 2023; revised 9 November 2023; accepted 28 November 2023; published 14 December 2023)

The discovery of built-in and synthetic Rashba fields in Si spin channels [S. Lee *et al.*, *Nat. Mater.* **20**, 1228 (2021)] challenged the conventional understanding of spin transport physics in semiconducting materials and forced researchers to reconsider the procedures used for estimating spin drift velocity and spin mobility. A conventional procedure for the estimation involves the detection of the Hanle-type spin precession under the application of an external magnetic field perpendicular to the plane; however, the in-plane effective magnetic fields due to the built-in Rashba fields hamper precise estimation because of the additional spin precession. In this work, we establish a precise method to estimate spin drift velocity and spin mobility, in addition to the spin lifetime and spin diffusion constant, by appropriately tuning the Rashba fields. Beyond the emblematic case of Si, the established method can be applied to other semiconductors, such as Ge and GaAs.

DOI: [10.1103/PhysRevB.108.214414](https://doi.org/10.1103/PhysRevB.108.214414)

I. INTRODUCTION

Semiconductor spintronics has been attracting significant attention because of the abundant spin physics, such as long spin coherence [1,2], gate tunability of spin transport [3,4], the first prediction and observation of the spin Hall effect [5,6], and the appearance of characteristic spin textures due to the spin-orbit interactions resulting in persistent spin helix [7,8]. Accordingly, the practical application of semiconductor spin physics in spin devices, such as spin transistors [9–12], also receives significant attention. Among spin transistors, spin metal-oxide-semiconductor field-effect transistors (MOSFETs) using group-IV elements [11], known as Sugahara–Tanaka-type spin transistors, play one of the pivotal roles in semiconductor spin devices because they enable energy-efficient and reconfigurable logic circuits by controlling both conductivity using a gate electric field and magnetoresistance using an external magnetic field. Notably, Si is regarded as the most promising material platform for the study and application of spin MOSFETs because of its ubiquity and lattice inversion symmetry, facilitating suppression of the spin-orbit interaction and the realization of long spin coherence.

The performance of spintronic devices is determined by their spin transport behavior, and numerous studies have focused on spin lifetime, spin diffusion constant and length, and spin mobility. Note that spin drift is inherently significant in semiconductor spin devices because a non-negligible electric field is applied for spin transport in semiconductors, unlike in metallic materials. Several studies have attempted to clarify the physics of spin drift in semiconducting materials, such as graphene [13] and Si [14–16], and enhancement of the spin transport length scale by applying an electric field has been experimentally demonstrated. A conventional approach

for investigating spin drift physics is to measure Hanle-type spin precession by simultaneously applying an external perpendicular magnetic field and a source-drain bias electric field using the local two- [16] or three-terminal [17] method with two ferromagnetic (FM) electrodes, where a conventional fitting function for the Hanle precession [18] is modulated to consider the contribution of the spin drift velocity v_s . However, the built-in and synthetic Rashba fields, which were first observed in Si MOS channels under the application of a gated electric field, affects the precise estimation of the spin lifetime and spin drift velocity [19]. The origin of the built-in Rashba field is the broken spatial inversion symmetry at the Si/SiO₂ interface in a spin MOSFET, and more importantly, the Rashba field is controllable by a gate voltage due to its electric field yielding an effective magnetic field as the synthetic Rashba field. The Rashba field invokes the in-plane effective magnetic field B_{eff} , which is perpendicular to both directions of the k vector of the moving spins in the Si channel and the spatial inversion breaking. Thus, precise estimation of the spin drift velocity is hampered because the B_{eff} induces additional spin precession, and the conventional approach must be revised.

In this paper, we report on the establishment of a precise method to estimate spin drift velocity and spin mobility in nondegenerate Si. The key is to suppress the B_{eff} due to the built-in Rashba field by determining the appropriate gate electric field. Under the proper conditions, the Hanle-type spin precession is simply caused by the external perpendicular magnetic field, and the conventional fitting function is valid for estimating the spin lifetime and spin drift velocity. The role of the built-in and synthetic Rashba fields in spin precession is discussed by comparing the results on spin lifetime anisotropy in nondegenerate and degenerate Si spin channels.

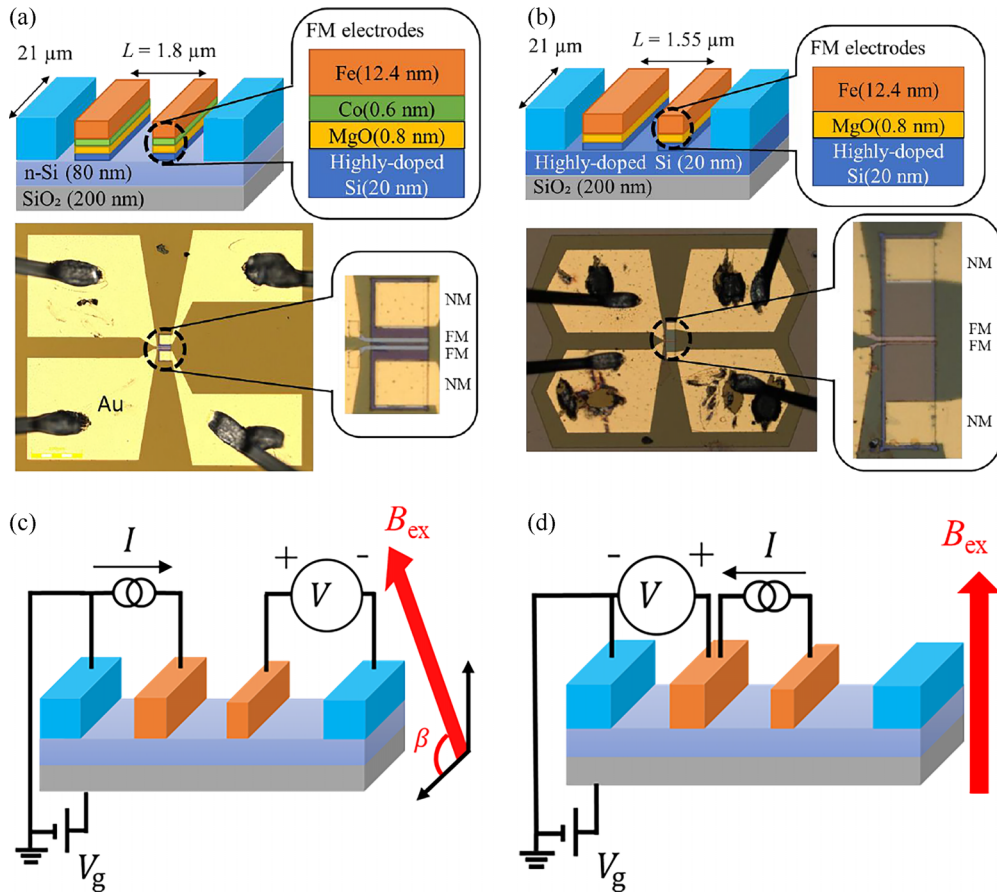


FIG. 1. Schematic and top optical microscopic images of device structures for (a) nondegenerate n -type Si and (b) degenerate n -type Si. Schematic images of measuring setups for the (c) nonlocal four-terminal oblique Hanle measurement and (d) local three-terminal Hanle measurement.

II. EXPERIMENT

Figures 1(a) and 1(b) show schematic and top optical microscopic images of the samples used in this study. The Si spin channels consist of nondegenerate and degenerate n -type Si, formed on 200-nm -thick SiO_2 . The thickness and width of the nondegenerate (degenerate) Si channel are 80 nm (100 nm) and $21 \mu\text{m}$ ($21 \mu\text{m}$), respectively, and the Si channels were formed by mesa etching. The gate voltages used to control the synthetic Rashba field are applied from the backside of the SiO_2 insulator (i.e., a back-gate spin MOSFET). The carrier density of the nondegenerate (degenerate) Si channel is $2 \times 10^{18} \text{ cm}^{-3}$ ($1 \times 10^{20} \text{ cm}^{-3}$). Two FM electrodes and two nonmagnetic (NM) electrodes are equipped with the Si channel. The FM electrode used for nondegenerate Si consists of a bilayer of Fe and Co, whereas only Fe is used for degenerate Si. The 0.8-nm -thick MgO tunneling barrier, in addition to the highly doped degenerate Si layer, is inserted between the FM electrode and the Si spin channel to avoid conductivity mismatch (for more details, see Fig. 1). The Fe/Co/MgO trilayer was formed by molecular beam epitaxy growth after rinsing the Si surface by hydrofluoric acid solution. The center-to-center length between the FM electrodes in the degenerate (nondegenerate) Si is $1.8 \mu\text{m}$ ($1.55 \mu\text{m}$). Figure 1(c) shows the setup of the oblique nonlocal four-terminal (NL4T) Hanle measurement used for studying the spin

lifetime anisotropy due to the synthetic Rashba field [20], where an external magnetic field B_{ex} is applied while tilting its angle β with respect to the Si channel plane under an applied gate voltage V_g . Note that the oblique NL4T Hanle measurement was only performed at $V_g = 0 \text{ V}$ for nondegenerate Si because the resistivity of degenerate Si is immune to an applied gate voltage. The oblique Hanle measurement helps with clarifying the spin lifetime anisotropy ratio ζ as a function of V_g , where ζ is the ratio of the spin lifetimes parallel (τ_s^{\parallel}) and perpendicular (τ_s^{\perp}) to the Si spin channel plane. An electric current I flows between a set of FM and NM electrodes and a voltage is measured between the other set of FM and NM electrodes [see Fig. 1(c)]. As aforementioned, spin drift velocity can be precisely estimated once ζ is controlled to be unity. Hence, the local three-terminal (L3T) Hanle measurement [17] under zero effective magnetic field enables estimation of spin drift velocity because an electric field is applied to the Si spin channel. Figure 1(d) shows the setup for the measurements, where the I flows between two ferromagnets, and spin accumulation beneath the downstream side ferromagnet is measured as the spin voltage. The B_{ex} is applied perpendicular to the Si channel. Keithley2010 (multimeter), Keithley2401 (source meter), Keithley2400 (source meter, for applying gate voltages), and DC current source (KIKUSUI) for magnetic field generation are exerted. All measurements are performed at room temperature.

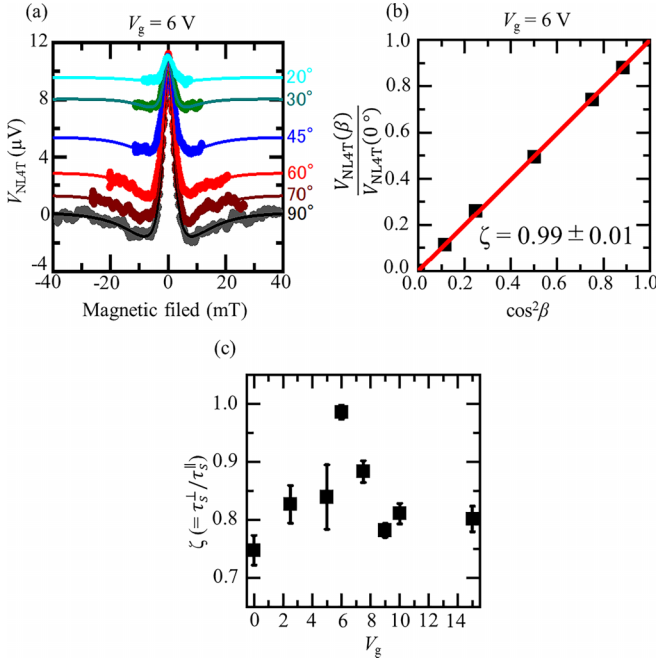


FIG. 2. (a) Results of the nonlocal four-terminal oblique Hanle measurement for various β in nondegenerate n -type Si. Solid lines show fitting results using the conventional fitting function for the Hanle-type spin precession (see also [21]). (b) The normalized spin voltages for various β as a function of $\cos^2\beta$. The red solid line shows the fitting result obtained using Eq. (1). (c) The V_g dependence of the spin lifetime anisotropy ratio ζ in nondegenerate n -type Si.

III. RESULTS AND DISCUSSION

The nonlocal oblique Hanle measurements are performed to determine the V_g , where the B_{eff} due to Rashba spin-orbit interaction is suppressed and the spin lifetimes, τ_s^{\parallel} and τ_s^{\perp} , are isotropic. Figure 2(a) shows the spin voltages obtained in the NL4T Hanle measurements, V_{NL4T} , for the nondegenerate n -type Si channel with various β (20° , 30° , 45° , 60° , 70° , and 90°) using $V_g = 6$ V and $I = -400$ μA . The results are well fitted using a conventional fitting function [18]. Since the precessional motion of spins dephases at $B_{\text{ex}} > 40$ mT, the dephasing spin voltage as a function of β , $V_{\text{NL4T}}(\beta)$, is determined by the remanent nonprecessional spin component along the B_{ex} direction, as observed in previous studies [19,20]. The angular dependence of the dephasing spin voltage normalized by that under $\beta = 0^\circ$ [21] is represented as

$$\begin{aligned} & \frac{V_{\text{NL4T}}(\beta)}{V_{\text{NL4T}}(0^\circ)} \\ &= \cos^2\beta \sqrt{\left[\cos^2\beta + \frac{1}{\zeta}\sin^2\beta\right]^{-1}} \\ & \times \exp\left(-\frac{L}{\sqrt{\tau_s^{\parallel}D_s}}\left(\sqrt{\left[\cos^2\beta + \frac{1}{\zeta}\sin^2\beta\right]} - 1\right)\right), \end{aligned} \quad (1)$$

where L is the center-to-center distance between two ferromagnetic electrodes, D_s is the spin diffusion constant, and ζ

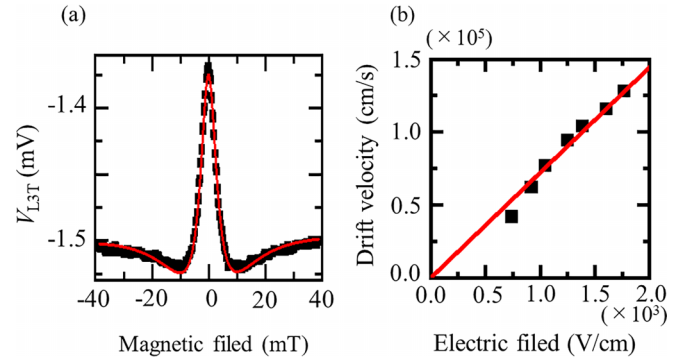


FIG. 3. (a) Results of the local three-terminal Hanle measurement using $I = 200$ μA and $V_g = 6$ V in nondegenerate Si, where the Rashba field is fully suppressed. The red solid line shows the fitting result obtained using Eq. (4). (b) The source-drain electric field dependence of spin drift velocity. The red solid line shows the linear fitting used to extract spin mobility.

is $\tau_s^{\perp}/\tau_s^{\parallel}$ as described above. Figure 2(b) shows the normalized dephasing spin voltage as a function of $\cos^2\beta$, where ζ is determined using Eq. (1). As a result, ζ is estimated to be unity (0.99 ± 0.01), indicating that the spin lifetime is isotropic and the B_{eff} is sufficiently suppressed under the applied V_g of 6 V. The whole dataset of ζ for various V_g is shown in Fig. 2(c). Under the zero gate electric field, ζ is 0.75 ± 0.02 , which signifies the existence of the built-in Rashba field [19]. As the gate voltage increases, ζ approaches unity at $V_g = 6$ V and then deviates from unity when V_g exceeds 6 V. The observed gate dependence is interpreted as follows: Up to 6 V, the applied gate voltage plays a role to suppress a built-in electric field. Above 6 V, the applied gate voltage creates an electric field, which is the summation of the built-in and the gate electric fields, and the sign of the total electric field is opposite to the original built-in electric field. However, the synthetic Rashba field is still in plane (although the sign of the Rashba field is reversed) and plays a role to give rise to spin lifetime anisotropy. The gate voltage dependence of the spin lifetime anisotropy shown in Fig. 2(c) is fully explained by the picture, which unequivocally shows the synthetic Rashba field is successfully suppressed. Indeed, the general trend of the result shown in Fig. 2(c) is consistent with that reported previously [19], also indicating that the built-in Rashba field in the Si is efficiently suppressed by the application of a suitable V_g . More importantly, the result unequivocally shows that the platform for precise estimation of spin drift velocity is established when the $V_g = 6$ V is applied for the device.

Figure 3(a) shows the result of the Hanle-type spin precession measurement using the L3T method under $I = 200$ μA (an electric field of 1×10^3 V/cm) and $V_g = 6$ V. In this setup, the spin-polarized electrons propagate in the Si by drift and diffusion, and the spin drift-diffusion equation described by Eq. (2) governs the spin motion in the conventional one-dimensional model [22,23],

$$\frac{\partial S}{\partial t} = D_s \frac{\partial^2 S}{\partial x^2} + v_s \frac{\partial S}{\partial x} - \frac{S}{\tau_s}, \quad (2)$$

where S is the spin density defined by a function of position x and time t , and τ_s is the intrinsic spin lifetime in the Si. An

analytical fitting function derived from Eq. (2) for the spin voltage in the steady state, V_{L3T} , divided by the I is described as [14]

$$\begin{aligned} \frac{V_{L3T}(B_{\text{ex}})}{I} = & \pm \frac{P^2 \sqrt{D_s T}}{2\sigma A} \exp\left(\frac{Lv_s}{2D_s}\right) (1 + \omega^2 T^2)^{-1/4} \\ & \times \exp\left[-\frac{L}{\sqrt{D_s T}} \left(\sqrt{\frac{\sqrt{1 + \omega^2 T^2} + 1}{2}}\right)\right] \\ & \times \cos\left[\frac{\tan^{-1}(\omega T)}{2} + \frac{L}{\sqrt{D_s T}} \sqrt{\frac{\sqrt{1 + \omega^2 T^2} - 1}{2}}\right], \end{aligned} \quad (3)$$

$$\left(T^{-1} = \frac{v_s^2}{4D_s} + \frac{1}{\tau_s}\right),$$

where P is the spin polarization, σ is the conductivity of the Si channel, A is the cross-sectional area of the Si channel, $\omega = g\mu_B B_{\text{ex}}/\hbar$ is the Larmor frequency, g is the g factor of an electron ($g = 2$ in this study), μ_B is the Bohr magneton, and \hbar is the Dirac constant [see also the details of the derivation of Eq. (3) in Ref. [3]]. Note that the spin drift velocity v_s is included in T and quantitatively estimated from the fitting. The experimental results are well fitted by Eq. (3) [see Fig. 3(a)], and v_s is estimated as $(7.7 \pm 0.1) \times 10^2$ m/s, where τ_s and D_s are set to be 2.8 ns and $6.9 \text{ cm}^2/\text{s}$, respectively, which are determined by the result of the nonlocal four-terminal measurement under $V_g = 6 \text{ V}$ and $\beta = 90^\circ$ [21]. To estimate spin mobility in nondegenerate Si, the magnitudes of the electric current are changed to control the electric field E , and the E dependence of v_s is plotted [see Fig. 3(b)], where the slope of the linear fitting line is the spin mobility μ_s in the Si. Thus, μ_s is estimated to be approximately $72 \text{ cm}^2/\text{V s}$, where the τ_s (2.8 ns) and D_s ($6.9 \text{ cm}^2/\text{s}$) are postulated to be the same under various electric fields because the applied electric field to the Si channel is 0.1–1 kV/cm and small enough to modulate them. Indeed, whereas some literatures reported bias electric field dependence of spin lifetime and diffusion constant in Si [24] and III-V semiconductor [25], magnitudes of the electric field in the Si and III-V semiconductors are 0.1–1 MV/cm and 10 kV/cm, respectively, and they are one to three orders of magnitude greater. Thus, our assertion that the spin lifetime and diffusion constant are almost unchanged can be concurred. Notably, the charge mobility of Si with the same carrier concentration was reported to be approximately $200 \text{ cm}^2/\text{V s}$ [26], which exhibits about threefold discrepancy with the charge and the spin mobilities. Further investigation is needed to explain this discrepancy in charge mobility, but the comparably small spin mobility may be due to the surface roughness of the thin Si layer and/or the spin Coulomb drag effect, as reported in graphene [27] and GaAs/AlGaAs [28].

Finally, we discuss how the built-in Rashba field affects spin precession in nonmetallic materials by measuring the Hanle-type spin precession in degenerate Si. Figures 4(a) and 4(b) show the results of the NL4T oblique Hanle measurements for degenerate Si. The tilting angles of the external magnetic field are varied ($\beta = 30^\circ, 45^\circ, 60^\circ, 70^\circ,$ and 90°) under $I = 1 \text{ mA}$. As mentioned previously, V_g is not applied to degenerate Si because the conductivity of degenerate

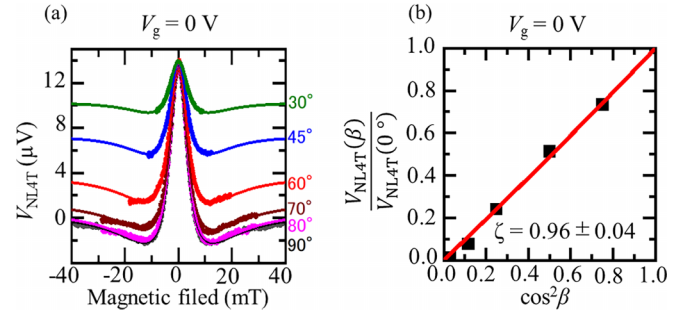


FIG. 4. (a) Results of the nonlocal four-terminal oblique Hanle measurement for various β in degenerate n -type Si. Solid lines show fitting results using the conventional fitting function for the Hanle-type spin precession (see also [21]). (b) The normalized spin voltages for various β as a function of $\cos^2 \beta$. The red solid line shows the fitting result obtained using Eq. (1).

semiconductors is unchanged by gating. Typical Hanle signals are obtained and the signals are well fitted by the fitting function [18] as in the case of the nondegenerate Si spin devices. The $V_{\text{NL4T}}(\beta)$ normalized by that at $\beta = 0^\circ$ [21] as a function of $\cos^2 \beta$ is shown in Fig. 4(b), where ζ is estimated to be approximately unity (0.96 ± 0.04), as in the result of the nondegenerate Si under $V_g = 6 \text{ V}$. Thus, the built-in Rashba field is negligibly small for the degenerate Si, unlike in nondegenerate Si (i.e., the effective magnetic field due to the Rashba field does not manifest itself in degenerate Si). Given that the back-gate voltage does not affect the interfacial resistance of the MgO/Si at the top electrode contact, according to the previous study [19], the synthetic Rashba field is dominant at the Si/SiO₂ interface. Hence, the results of the nondegenerate and degenerate Si in this study signify that interfacial band bending at the nondegenerate Si/SiO₂ interface gives rise to a built-in electric field, and the built-in Rashba field and band bending are not observed in degenerate Si. Overall, the results bear out that the built-in and the synthetic Rashba field should be considered in nondegenerate semiconductor spin devices to realize precise estimation of spin transport physics in them.

IV. SUMMARY

In this study, we have established a method for quantitatively and precisely estimating spin drift velocity and spin mobility in a nondegenerate Si spin MOSFET. By applying a suitable gate voltage, the built-in Rashba field in Si due to the electric field at the Si/SiO₂ is efficiently suppressed. Under the gate voltage application, the source-drain electric field is applied to invoke spin drift in nondegenerate Si, and under the appropriate condition (i.e., a suitable gate voltage), the Hanle-type spin precession measurement can be conducted to precisely estimate the spin drift velocity and spin mobility in the Si, in addition to spin lifetime. Beyond the emblematic case of Si, the established method is applicable to other semiconductors, such as Ge and GaAs.

ACKNOWLEDGMENTS

A part of this study was supported by a Grant-in-Aid for Scientific Research (A), “Creation of high performance

Si spin transistors and development of spin calculation functions” (Grant No. 21H04561) and MEXT Initiative to

Establish Next-Generation Novel Integrated Circuits Centers (X-nics, Tohoku University).

-
- [1] X. Lou, C. Adelmann, S. A. Crooker, E. S. Garlid, J. Zhang, K. S. Madhukar Derry, S. D. Flexner, C. J. Palmstrom, and P. A. Crowell, *Nat. Phys.* **3**, 197 (2007).
- [2] T. Suzuki, T. Sasaki, T. Oikawa, M. Shiraishi, Y. Suzuki, and K. Noguchi, *Appl. Phys. Express* **4**, 023003 (2011).
- [3] T. Sasaki, Y. Ando, M. Kameno, T. Tahara, H. Koike, T. Oikawa, T. Suzuki, and M. Shiraishi, *Phys. Rev. Appl.* **2**, 034005 (2014).
- [4] S. Lee, F. Rortais, R. Ohshima, Y. Ando, M. Goto, S. Miwa, Y. Suzuki, H. Koike, and M. Shiraishi, *Appl. Phys. Lett.* **116**, 022403 (2020).
- [5] S. Murakami, N. Nagaosa, and S.-C. Zhang, *Science* **301**, 1348 (2003).
- [6] Y. K. Kato, R. C. Myers, A. C. Gossard, and D. D. Awschalom, *Science* **306**, 1910 (2004).
- [7] M. Kohda, V. Lechner, Y. Kunihashi, T. Dollinger, P. Olbrich, C. Schönhuber, I. Caspers, V. V. Bel’kov, L. E. Golub, D. Weiss, K. Richter, J. Nitta, and S. D. Ganichev, *Phys. Rev. B* **86**, 081306(R) (2012).
- [8] A. Sasaki, S. Nonaka, Y. Kunihashi, M. Kohda, T. Bauernfeind, T. Dollinger, K. Richter, and J. Nitta, *Nat. Nanotechnol.* **9**, 703 (2014).
- [9] B. Das and S. Datta, *Appl. Phys. Lett.* **56**, 665 (1990).
- [10] H. C. Koo, J. H. Kwon, J. Eom, J. Chang, S. H. Han, and M. Johnson, *Science* **325**, 1515 (2009).
- [11] S. Sugahara and M. Tanaka, *Appl. Phys. Lett.* **84**, 2307 (2004).
- [12] T. Tahara, H. Koike, M. Kameno, T. Sasaki, Y. Ando, K. Tanaka, S. Miwa, Y. Suzuki, and M. Shiraishi, *Appl. Phys. Express* **8**, 113004 (2015).
- [13] C. Jozsa, M. Popinciuc, N. Tombros, H. T. Jonkman, and B. J. van Wees, *Phys. Rev. Lett.* **100**, 236603 (2008).
- [14] B. Huang, D. J. Monsma, and I. Appelbaum, *Phys. Rev. Lett.* **99**, 177209 (2007).
- [15] M. Kameno, Y. Ando, E. Shikoh, T. Shinjo, T. Sasaki, T. Oikawa, Y. Suzuki, T. Suzuki, and M. Shiraishi, *Appl. Phys. Lett.* **101**, 122413 (2012).
- [16] M. Kameno, Y. Ando, T. Shinjo, H. Koike, T. Sasaki, T. Oikawa, T. Suzuki, and M. Shiraishi, *Appl. Phys. Lett.* **104**, 092409 (2014).
- [17] T. Sasaki, T. Suzuki, Y. Ando, H. Koike, T. Oikawa, Y. Suzuki, and M. Shiraishi, *Appl. Phys. Lett.* **104**, 052404 (2014).
- [18] T. Sasaki, T. Oikawa, T. Suzuki, M. Shiraishi, Y. Suzuki, and K. Noguchi, *IEEE Trans. Magn.* **46**, 1436 (2010).
- [19] S. Lee, H. Koike, M. Goto, S. Miwa, Y. Suzuki, N. Yamashita, R. Ohshima, E. Shigematsu, Y. Ando, and M. Shiraishi, *Nat. Mater.* **20**, 1228 (2021).
- [20] B. Raes, J. E. Scheerder, M. V. Costache, F. Bonnel, J. F. Sierra, J. Cuppens, J. Van de Vondel, and S. O. Valenzuela, *Nat. Commun.* **7**, 11444 (2016).
- [21] See Supplemental Material at <http://link.aps.org/supplemental/10.1103/PhysRevB.108.214414> for the nonlocal spin voltages for the nondegenerate and degenerate Si, the analysis of the nonlocal four-terminal Hanle measurements, and the angular dependence of the normalized dephasing spin voltages under various gate voltages.
- [22] Z. G. Yu and M. E. Flatté, *Phys. Rev. B* **66**, 201202(R) (2002).
- [23] Z. G. Yu and M. E. Flatte, *Phys. Rev. B* **66**, 235302 (2002).
- [24] S. Sato, M. Ichihara, M. Tanaka, and R. Nakane, *Phys. Rev. B* **99**, 165301 (2019).
- [25] G. Wang, B. L. Liu, A. Balocchi, P. Renucci, C. R. Zhu, T. Amand, C. Fontaine, and X. Marie, *Nat. Commun.* **4**, 2372 (2013).
- [26] *Quick Reference Manual for Semiconductor Engineers*, edited by W. F. Beadle, J. C. C. Tsai, and R. D. Plummer (Wiley, New York, 1985).
- [27] T. Maassen, J. J. van den Berg, N. Ijbema, F. Fromm, T. Seyller, R. Yakimova, and B. J. van Wees, *Nano Lett.* **12**, 1498 (2012).
- [28] C. P. Weber, N. Gedik, J. E. Moore, J. Orenstein, J. Stephens, and D. D. Awschalom, *Nature (London)* **437**, 1330 (2005).